

## STRAIN ANALYSIS OF A PRESSURE VESSEL TEST SPECIMEN CONTAINING METAL LOSS DEFECTS

Leonardo Dantas Rodrigues, leodr@prima7s.com  
José Luiz de França Freire, jlfreire@puc-rio.br  
Ronaldo Domingues Vieira, rdvieira@puc-rio.br  
Jaime Tupiassú Pinho de Castro, jtcastro@puc-rio.br  
Pontifícia Universidade Católica do Rio de Janeiro, PUC-Rio

**Abstract.** *This investigation applied the digital image correlation technique – DIC – to a thin walled cylindrical vessel that contained four (two longitudinal and two circumferential) metal loss defects. The DIC has proven to be a good choice for this type of experiment, where elastic and plastic surface strains need to be measured. The uncertainty of the DIC technique was assessed by measuring strain fields induced by opening soft drink beverage cans and by comparing DIC results with electrical resistance strain gage measurements. Using the equations proposed by DNV RP F-101 and by Kastner, the investigation also addressed the calculation of the burst pressure of a cylindrical vessel with simulated corrosion defects. Results showed that the longitudinal elastic strains or stresses acting on the defects of the tested vessel could be well predicted by the Kastner equation; and also that the circumferential strains and stresses measured in the defect patches were higher than the values predicted by the DNV equation. On the other hand, the actual burst pressure of the vessel tested was conservatively (20% lower) and reasonably well predicted by the DNV equation.*

**Keywords:** *pressure vessels, pipelines, corrosion defects, strain gages, digital image correlation*

### 1. INTRODUCTION

This investigation had two objectives. The first was to apply the digital image correlation technique – DIC – (Yoneyama and Murasawa, 2009) to a cylindrical pressure vessel containing metal loss defects. The DIC technique has proven to be useful for this type of experiment, where elastic and plastic surface strains need to be measured. Its main advantages are ease of specimen preparation, robust adequacy for different and harsh test conditions, and full field capacity. The second objective was to verify the prediction of cylindrical vessels burst pressure by the DNV-RP-F101 (2004) and by the Kastner *et al.* (1981) equations, frequently used for determining burst pressures and stresses in the circumferential and longitudinal directions of thin walled cylinders such as pressure vessels, pipes and pipelines that are loaded by internal pressure and contain metal loss defects.

To start with, the DIC method is briefly introduced, and an uncertainty analysis of its strain response is developed by means of simple laboratory tests that employ pop-top aluminum beverage cans as test specimens. Next, the elastic-plastic strain and burst pressure data determined for one pressure vessel - PV - tubular test specimen is analyzed. This specimen was cut from a longitudinally welded tube made of low carbon steel with a nominal outside diameter of 76.2 mm (3 in) and a nominal wall thickness of 2.04mm. The PV specimen had two longitudinal and two circumferential metal loss defects machined into its external surface. These defects were placed in pairs symmetrically located along the specimen. First, the PV was loaded and then unloaded under elastic conditions (adjusting its internal pressure such that plasticity just started to develop in its most strained area.) Two techniques were used to measure the elastic strains induced by this load: electrical resistance strain gages and DIC. Next, the PV specimen was reloaded from zero pressure up to burst pressure. During this second test, elastic and plastic strains were continuously measured with the strain gages (up to the point that the most strained gages stopped responding.) The DIC technique was applied in the second experiment after the bursting and the automatic unloading of the specimen in order to determine the final remaining strains in the defect areas that had not suffered fracture.

The results obtained from the uncertainty evaluation and the PV tests allowed conclusions regarding the use of small pop-top beverage cans to determine the uncertainty of the DIC technique. Such results validate the DIC use in elastic and plastic strain measurements of pipeline and vessel specimens on surface areas that have suffered metal loss due to corrosion or erosion damage mechanisms. From them the application of analytical equations published by DNV RP-F101 and by Kastner for determining the burst pressure and the circumferential and longitudinal stresses occurring in the metal loss defect areas of cylindrical vessels could be evaluated. Using this information, a forthcoming study will investigate the validity of applying the Tresca and the Mises criteria to the ductile rupture of thin walled cylindrical vessels under internal pressure.

## 2. CYLINDRICAL PRESSURE VESSELS WITH LONGITUDINAL AND CIRCUMFERENTIAL DEFECTS

Over the past decade, over forty full scale burst tests have been conducted by PETROBRAS and PUC-Rio to investigate the failure behavior of pipelines containing corrosion defects. Several types of corrosion defects have been tested, namely short and long longitudinal defects, uniform depth defects, non uniform depth defects, simulated defects (machined using spark erosion), real defects (removed from service) and colonies of defects. Most of these tests have already been published and are referenced in “Benjamin et al. (2010)” and “Freire et al. (2011)”. This later reference also includes a list of reduced scale test specimens.

Recently, the burst tests of six tubular specimens loaded by internal pressure (Benjamin et al, 2010 and 2009) were analyzed by “Freire et al (2011)” in terms of strain distributions determined by strain gages located inside the corrosion patches and in terms of the adequacy of failure pressure predictions. These predictions are based on simple equations proposed in the literature for corrosion geometries that are localized in a transition zone, which can be classified as short longitudinal defects or long circumferential defects. The test specimens reported in “Benjamin et al 2010 and 2009” were cut from longitudinally welded tubes made of API 5L X80 steel with a nominal outside diameter of 457.2 mm (18 in) and a nominal wall thickness of 7.93 mm (0.312 in). Each of the six specimens had one external longitudinal or circumferential corrosion defect that had been machined using spark erosion. Tensile and impact test specimens cut from the same tubes were tested to determine material properties. Post-yielding strain gages were used to measure the elastic and plastic strains. The failure pressures measured in the tests were compared with those predicted by the DNV RP-F101 method for single defects and by the Kastner equation. The results confirmed that, depending on the dimensions of a corrosion defect ( $d$ ,  $L$  and  $w$  – respectively depth, length and width of the metal loss), failure is governed either by the circumferential (hoop) stress or by the longitudinal stress. The longitudinal direction of a fracture caused by a defect suggests that the failure is governed by the hoop stress. The strain distributions measured for points inside the corrosion patches would also indicate the same trend: the much larger circumferential strains imply longitudinal fractures, and the much larger longitudinal strain implies a circumferential fracture.

Assuming that the pipeline or pressure vessel is a thin shell (ratio of the pipeline’s outside diameter  $D_e$  to the pipeline’s wall thickness  $t$  is greater than twenty ( $(D_e/t) \geq 20$ )), the radial stress  $\sigma_r$  at any point of the pipe wall is negligibly small. Consequently there are only two stresses at any point of the pipe wall: the hoop or circumferential stress  $\sigma_c$  and the longitudinal stress  $\sigma_l$ . The hoop tensile stress  $\sigma_c$  and the longitudinal tensile stress  $\sigma_l$  are related to the internal pressure  $p$  by equations (1-2) for points of the thin pipe located in nominal regions, i.e., located far away from the defect patches and from the pipe caps:

$$\sigma_c = p \frac{D}{2t} \quad (1)$$

$$\sigma_l = n \sigma_c \quad (2)$$

where  $n = 0.5$  or  $n = \nu = 0.3$  respectively, are associated to longitudinally unrestrained pipes or to longitudinally restrained pipes,  $\nu$  being the Poisson’s coefficient.

In a pipeline subjected only to internal pressure, the nominal circumferential stress  $\sigma_c$  and the nominal longitudinal stress  $\sigma_l$  are positive (tensile stress). Thus, the equations of the Tresca failure criterion are:

$$\sigma_c = \sigma_{flow} (f_R)_c \quad (3)$$

or

$$\sigma_l = \sigma_{flow} (f_R)_l \quad (4)$$

where  $\sigma_{flow}$  is the material flow stress and  $(f_R)_c$  and  $(f_R)_l$ , respectively, are the reduction strength factors in the circumferential and longitudinal directions caused by the corrosion defect’s geometry. The reduction factor in the circumferential direction  $(f_R)_c$  is given by equation (5). Table 2 of “Benjamin et al (2010)” presents the equations adopted by four selected methods to calculate flow stress  $\sigma_{flow}$ , pipe diameter  $D$ , geometric factor  $\alpha_{area}$  and bulging factor  $M$ . Other variables in these equations are maximum depth of corrosion  $d$  and length  $L$  and width  $w$  of the corrosion patch. The equations used by DNV-F101 for  $\alpha_{area}$  and  $M$  are given in equation (5), and  $\sigma_{flow}$  is equal to the material’s ultimate strength,  $S_u$ . The reduction factor in longitudinal direction  $(f_R)_l$  was derived by Kastner and is given in equation (6). Angle  $\beta$  is the half angle width of the circumferential defect. The burst pressure based on the circumferential stress is given by equation (7). It is generally accepted that the best equation to represent the longitudinal stress in a corroded pipe at failure is given by equation (8).

$$(f_R)_c = \frac{1 - \alpha_{area} (d/t)}{1 - \alpha_{area} (d/t) M^{-1}} \quad \alpha_{area} = 1 \quad M = \sqrt{1 + 0.31 \frac{L^2}{D_e t}} \quad (5)$$

$$(f_R)_l = \frac{\left(1 - \frac{d}{t}\right) \left(\pi - \beta \frac{d}{t}\right)}{\pi \left(1 - \frac{d}{t}\right) + 2 \frac{d}{t} \sin \beta} \quad (6)$$

$$(p_f)_c = \sigma_{flow} \frac{2t}{D_e - t} \frac{1 - \alpha_{area} (d/t)}{1 - \alpha_{area} (d/t) M^{-1}} \quad (7)$$

$$(p_f)_l = \sigma_{flow} \frac{1}{n} \frac{2t}{D_e} \frac{\left(1 - \frac{d}{t}\right) \left(\pi - \beta \frac{d}{t}\right)}{\pi \left(1 - \frac{d}{t}\right) + 2 \frac{d}{t} \sin \beta} \quad (8)$$

In order to augment the number of data points and thus the confidence in the correctness of applying the DNV and Kastner equations, a number of new tests are proposed by the authors. In order to use two possible means of performing less expensive rupture tests, it was decided that the present investigation would be carried out using a reduced scale model of a pressure vessel specimen coupled with a new full field optical analysis technique that is able to determine small and large strains. These two possible means are coupled and investigated herein.

### 3. DIGITAL IMAGE CORRELATION

The advance of computer vision, hardware, software and modern numerical analysis methods of optical data have enabled a particular optical technique to flourish recently. This technique determines displacements of points that belong to the assessable surface of deformable solids or of points in suspension that belong to a fluid in movement. The name Digital Image Correlation (DIC) is commonly used when applying this technique to deformable solids, whereas Particle Image Velocimetry (PIV) is commonly applied to the study of two and three dimensional flow patterns.

The basic experimental setup of a three-dimensional DIC test is illustrated in Figures 1 and 2. The plane or curved surface of a body contains a pattern of randomly spaced points and is photographed using two digital CCD cameras before and after the load is applied to the body. Image correlation and analysis of both initial and final pictures enable the accurate determination of the u, v and w displacement fields that result from the body's deformation. Two-dimensional DIC requires only one CCD camera orthogonally oriented to the object's surface, but the distance of the object to the camera must not vary. Three-dimensional u, v, w displacement determination and analysis can be accomplished by the use of two CCD cameras in a stereographic arrangement. The images of dots (random pattern) introduced by painting (or similar technique) them on the surface of the deformable body are photographed by the CCD cameras and downloaded to the frame grabbing circuit that relates the intensity of light for each of the many pixels that form the image. Ideally, the dot's size fully covers one pixel and somewhat affects the light intensity of a group of 3x3 adjacent pixels. The density of about 1 dot for each square of 3x3 pixels leads to the use of subset sizing, for example 16x16 or 41x41 pixels that contain about and respectively 30 or 90 dots (Shukla and Dally, 2010). The technique aims to determine the average displacements of the subset centers between the initial and final images. The precise location of the center of the subset is acquired in the order of a fraction of pixel. Subset motion is determined when the selected subset of the un-deformed (first) image is identified in the deformed (second) image. Identification is accomplished by using a search algorithm that looks for the best correlation between distributions of light intensities of the un-deformed and of the deformed subset images.

Equation (9) shows one possible correlation function that can be used to identify the subset matching where  $F(x, y)$  and  $G(x^*, y^*)$  represent the gray levels (light intensities) of each point  $(x, y)$  or  $(x^*, y^*)$  inside the un-deformed or deformed subset. The best fit of matching is given by the maximum value of  $C$ . The cross-correlation is given by

$$C(x, y, x^*, y^*) = \frac{\sum F(x, y).G(x^*, y^*)}{\sqrt{\sum F(x, y)^2 \cdot \sum G(x^*, y^*)^2}} \quad (9)$$

The distribution of gray level from pixel to pixel is a discrete function. Continuous gray level distributions can be achieved for both images if the pixel by pixel gray level distributions can be smoothed out by some kind of interpolation function. The best search to achieve a maximum value for  $C$  or a minimum value for  $1 - C$  determines the coordinate pair  $(x^*, y^*)$  expressed by an approximating series, such that

$$\begin{aligned} x^* &= x + u + \frac{\partial u}{\partial x} \Delta x + \frac{\partial u}{\partial y} \Delta y + \dots \\ y^* &= y + v + \frac{\partial v}{\partial x} \Delta x + \frac{\partial v}{\partial y} \Delta y + \dots \end{aligned} \quad (10)$$

where only the linear terms were explicitly written. Achievement of the best correlation will provide the terms  $u, v, \frac{\partial u}{\partial x}, \frac{\partial v}{\partial x}, \frac{\partial u}{\partial y}, \frac{\partial v}{\partial y}$  that make possible the determination of the strain state  $\epsilon_x, \epsilon_y, \epsilon_{x,y}$ . In these cases, expressions for small or large strains can be used. Minimization of the expression  $1 - C(x, y, x^*, y^*)$  may be achieved by using the Newton-Raphson method (Sutton, Orteu and Schreier, 2009).

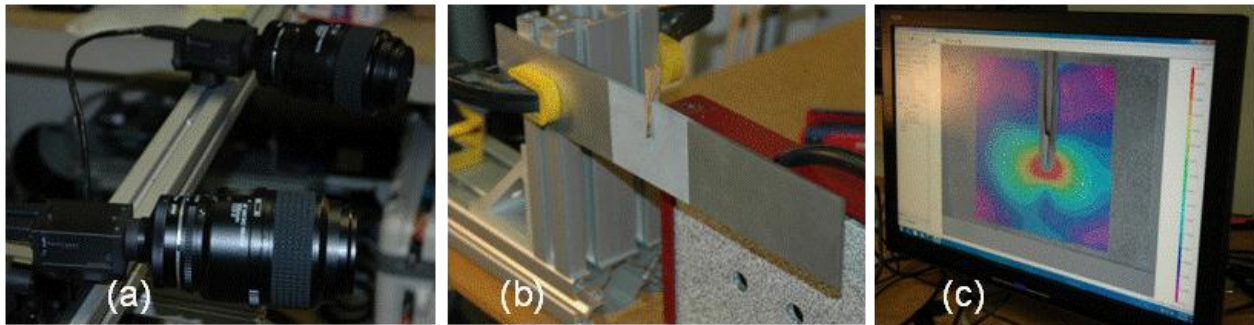


Figure 1: Essentials of the DIC technique: (a) two CCD cameras and two lenses mounted in a rigid support; (b) specimen at the testing bench showing applied random speckle pattern which will be viewed and photographed by the digital cameras; (c) high resolution screen showing image analyzed by the DIC software. Practice test run at Correlated Solutions (Columbia, SC, USA).

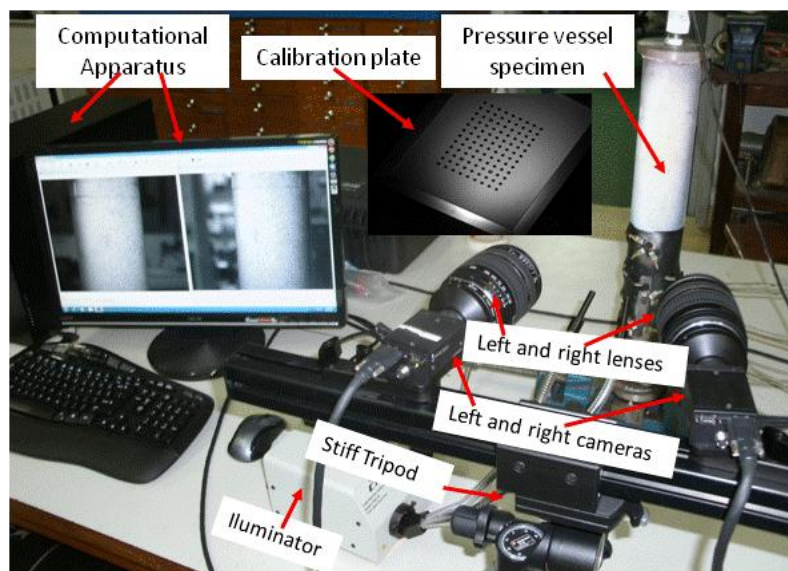


Figure 2: Thin walled cylindrical pressure vessel mounted in the DIC testing bench of PUC-Rio; the calibration template and fiber optic guided illuminator are showed in the picture.

Calibration of the stereo imaging system is achieved by using a speckle dot pattern mounted on a precision translation stage. Prior to an experiment, the stereovision system is calibrated using a target with uniformly spaced markers, which is tilted and rotated into different positions while pictures are being taken.

Typical hardware and image analysis software provided by commercial vendors nowadays can achieve an accuracy of about 0.01 pixels or better for in-plane displacements, and a point-by-point accuracy of  $\pm 100 \mu\epsilon$  for in-plane surface strains, if a gage length of about 200 pixels is adopted.

In this study, a quick practice test using pop-top aluminum beverage cans was devised to give quantitative practical information regarding the method's accuracy. This type of test is very common in strain gage training practices. It was easy to adapt the can test to the DIC training practice as well as to help in identifying the uncertainty of the DIC method in experiments that involve small pressure vessels. The can test entails bonding one or more electrical strain gages (or white painting followed by black dot painting) onto the cylindrical beverage can, registering the initial zero test state and then opening the can. Strain gage readings will be directly related to the elastic strains released by bringing the pressure down to zero. In the case of the 3D stereo DIC technique can test, initial and final photographs of the dots' distributions are taken and the images are analyzed to give displacement and strain distributions. Figure 3 shows details of the cans and of the pressure vessel specimens used.

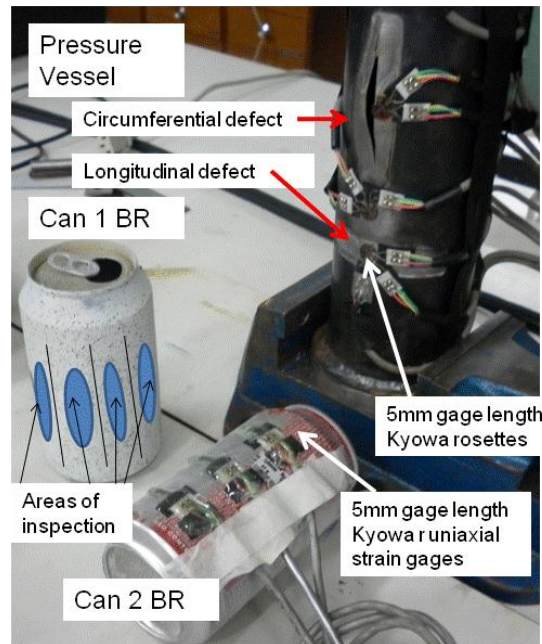


Figure 3: Pop-up beverage cans and strain gage instrumented part of the pressure vessel used in the present paper.

Beverage cans were instrumented with strain gages and/or painted with dots for the DIC tests. The results were used in the present uncertainty analysis and are summarized in Table 1. The data in Table 1 entail two sets of strain gage can tests performed at two different universities in Rio, one set of DIC tests performed at Correlated Solutions Inc. (Columbus, SC, USA) and two specific DIC tests performed at PUC-Rio, devised to enhance the assessment of uncertainty. One test analyzed 8 longitudinal areas of Can 1 BR covering its 360° contour. The second test (Can 2 BR) analyzed three areas of inspection with dimensions of about 15x15mm<sup>2</sup>. These areas were located along one generatrix of the can's body. These locations were positioned symmetrically on the sites where three electrical resistance strain gages were bonded to measure the circumferential strains released by the can upon opening it (see Figure 3).

Analysis of the data from all these tests is briefly summarized in Table 1. Basic uncertainties are assessed in terms of circumferential strains measured at various points on the cans and in terms of their comparisons with average values and standard deviations of the data collected. A judicious evaluation of the data presented in Table 1 leads to a number equal to ±100 µε or to a standard deviation of ±15% (whichever is larger) of the measured strain, to express the experiments' uncertainty. An additional way of expressing uncertainty might be a number equal to ±7% of the mean of at least 5 strain data points measured at locations close to each other where a quasi uniform state of strain is expected.

Figure 4 highlights results obtained with the can tests by presenting circumferential and longitudinal strain distributions determined by the DIC technique for points located along a circumferential line on Can 1 US. One can see a quite uniform behavior of these strain distributions. Two points should be commented on. The first calls attention to the fact that both strains are directly dependent on the thickness of the point being considered. Analysis performed on some of the aluminum cans revealed that thickness in the same specimen may vary up to 0.005mm from one point to another. The average thickness is equal to 0.10mm and the standard deviation of 20 points measured on the same can is 0.004mm. The second point refers to the ratio of the average of the measured values of  $\epsilon_l$  and  $\epsilon_c$  shown in the Figure. The ratio is equal to 0.20 and this value is the one expected for aluminum cans.

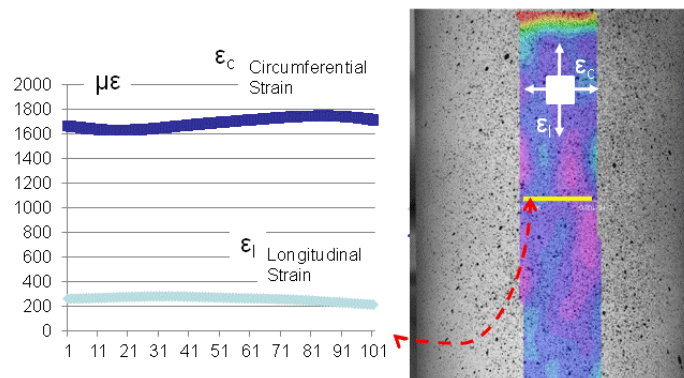


Figure 4: Circumferential and longitudinal strains plotted along 101 selected points that belong to the center line of the area of inspection of Can 1 US.

Table 1: Summary of analysis of uncertainty data collected with the SG and DIC techniques using soft drink cans

Test name	Comments	Technique details	Circumferential strain point or average data ( $\mu\epsilon$ )	Standard deviation ( $\mu\epsilon$ )	Coefficient of variation (%)	Further comments
PUC-Rio 2010-1	Tests performed with 10 different cans from same origin. Two results discarded using Chauvenet's criterion	Strain gages with 5mm gage length	1920	167	9	-
UERJ 2010-2	Tests performed on 8 different cans from same origin	Strain gages with 5mm gage length	1964	90	5	-
Can US 1	Tests performed at Correlated Solutions – USA on June 04 2010 – cans from the same origin. Center point data located in arbitrary 50x30mm <sup>2</sup> area of inspection	DIC – CS <sup>1</sup>	1680	-	-	Repetition of analysis encompassing 8 different data points on Can US 1 using two different photographs of data collection with a generated average error of -19 $\mu\epsilon$ and standard deviation of 31 $\mu\epsilon$
Can US 2		DIC – CS	1578	-	-	
Can US 3		DIC – CS	1639	-	-	
Can US 4		DIC – CS	1725	-	-	
Can BR 1	Tests performed at PUC-Rio – cans from the same origin.	DIC – PUC-Rio <sup>2,3</sup>	$\epsilon_c = 1989$	223	11	Center point data located on 8 (50x20mm <sup>2</sup> ) areas of inspection that attempted covering the entire body of the can. Center points for data collection were chosen by careful inspection.
			$\epsilon_i = 409$	124	30	
			$\epsilon_c = 1994$	134	7	
			$\epsilon_i = 400$	75	19	
Can BR 2 <sup>4</sup>		Strain gages with 5mm gage length	1918	161	8	Three strain gages located in the same generatrix. Reinforcing factor of 1.15 was considered due to epoxy adhesive protection located over installation site <sup>5</sup>
		DIC – PUC-Rio	1901	107	6	Three areas of inspection with 20x20mm <sup>2</sup> located in the same generatrix.
Notes	1- DIC – CS = Practice tests performed at Correlated Solutions in June, 2010					
	2- DIC – PUC-Rio = Practice tests performed at PUC-Rio in December, 2010					
	3- Can BR 1 had thickness measured at three points on each of 8 areas of inspection. Average thickness was 0.102mm and standard deviation was 0.005mm					
	4- Root mean square deviation among strain gages and DIC results for the three areas inspected was 94 $\mu\epsilon$					
	5- Factor calculated using force equilibrium equations; aluminum and epoxy Young modulus equal to 70GPa and 1.5GPa, respectively; section areas for each epoxy reinforcement equal to 3x7mm <sup>2</sup> ; section area of can corresponding to each reinforcement equal to 0.1x30mm <sup>2</sup>					

#### 4. PRESSURE VESSEL TESTS

The raw material used in the test was composed of one longitudinally welded pipe made of low carbon steel. The length of the original pipe was approximately 6m. The nominal outside diameter and the nominal wall thickness of the pipe were, respectively, 76.7mm and 2.04mm. The yield and ultimate strength were measured using a tubular vessel 600mm long fabricated from the same pipe and burst with internal pressure as reported in “Caylar (2009)”. The measured specimen's ultimate pressure and the calculated yield and ultimate strength (based on von Mises theory) were 22.6MPa, 293MPa and 366MPa, respectively.

The pressure vessel specimen was 600mm long, and had two circumferential defects and two longitudinal defects milled to simulate external and uniform depth corrosion (or erosion) defects. These defects were machined opposite to the tube seam weld. The defects were located in symmetrical positions relative to the ends of the specimens. The simulated corrosion defects were smooth rectangular defects, i.e., the shape of the longitudinal area of metal loss was rectangular with smooth edges. The tubular specimen was closed with plane heads that were welded on before the defects were machined. The specimen is presented in Figure 5 and the actual dimensions of each tubular specimen and respective defects are presented in Table 2. Machining of the defects was not exact enough to guarantee uniformity of the four defect depths along their lengths. Therefore, values given for the defect depths in Table 2 are valid for points near the center of the defects. The variation of the defect depths along the defects' lengths are in the order of  $\pm 0.1$ mm.



Using the values of ratios  $L^2/(D_e t)$ , one can see that the so called longitudinal and circumferential defects are, respectively, equivalent to long and short corrosion defects according to the ASME B31G method in “ASME (1991)” (defects are long if  $L > \sqrt{20 D_e t}$ , and short if  $L \leq \sqrt{20 D_e t}$ ).

Table 2 – Actual dimensions of the tubular specimens and of the machined defects

Defect	$t^*$ (mm)	$L$ (mm)	$w$ (mm)	$\beta$ ( $^\circ$ )	$\frac{d}{t}$	$\frac{L^2}{D_e t}$	$D_e = 76.7\text{mm}$ $t = 2.04\text{mm}$ $a1 = 70\text{mm}$ $a2 = 30\text{mm}$
Long-SG	0.88	80	15	11	0.57	41	
Circ-SG	0.92	15	82	61	0.55	1.4	
Long-DIC	1.19	80	15	11	0.42	41	
Circ-DIC	1.39	15	82	61	0.32	1.4	

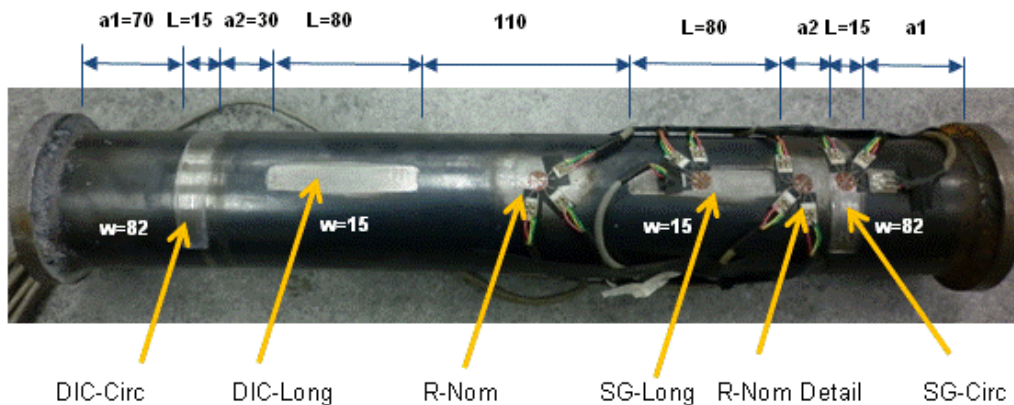


Figure 5: General view of the pressure vessel specimen, presenting the location of defects and strain gage rosettes

The PV specimen was loaded with internal pressure only. The water pressurizing system used an air driven pump with a maximum capacity of 70MPa. Test pressure was monitored with a Gefran manometer. Strain gage and manometer data readings were made with a Lynx ADS 2000 system. Strain gages rosettes were manufactured by Kyowa (KFC-5-120). A cyanoacrylate based adhesive was used. The strain gages were connected to the Lynx system using the traditional 3-wire arrangement. As expected, the most-strained gage stopped measuring after a total deformation of about 4% was reached. This occurred during the last (burst) test. The DIC technique was performed with a 3-D stereo Correlated Solutions system. The system consisted of two CCD cameras, two lenses, a tripod, calibration targets (4, 5 and 9mm were used in the tests), and two software – one for image acquisition (VIS-Snap 2009) and another for data analysis (VIC-3D 2009). Figure 2, 3 and 5 show the DIC hardware arrangement, the PV specimen and some of the beverage cans used in the tests.

Four pressure tests were performed. In the first three tests, pressure was increased from 0 to 5MPa in five steps. Strain gage readings and DIC images were taken at each step. In one of these tests both longitudinal and circumferential defects were visualized at the same time (global test). The second and third tests were performed in such a way that the defects were magnified in the pictures (local tests). In other words, the second test was performed with full vision of the longitudinal defect and the third test was performed with full vision of the circumferential defect.

The fourth test was performed in two steps. First, under zero pressure, initial images were taken from the global field that covered both defects. Next, the specimen was taken off the optical DIC bench and positioned inside the test bunker to be pressurized up to bursting. Rupture, as expected by the dimensions that resulted from the defect machining process, occurred in the area of the longitudinal defect with the smallest thickness (the one instrumented by the rosette). It should be noted that strain gage readings were taken during the bursting test up to the point the circumferential gage located in the center of the longitudinal defect stopped measuring, due to the very large strain reached. After bursting, the specimen was again positioned on the optical bench as close as possible to its previous (initial) position in order to be viewed and photographed again by the cameras. In this way it was possible to collect data to determine the remaining plastic strains that occurred in the defects' area covered by the DIC analysis. The image of the area viewed by one of the cameras used in the DIC analysis is presented in Figure 6.

Strain and pressure data collected during the four tests are presented in Figures 6 - 9 and in Table 3. Elastic strains measured by the strain gage and DIC techniques along with pressure variation are depicted in Figure 7a for the longitudinal defect areas. Only the circumferential strains are presented in this Figure due to the fact that they were much larger than the longitudinal strains in all tests. All circumferential strain gage and DIC determined data are plotted in Figure 7b for comparison purposes. At this point it is important to note that the DIC data presented in Figure 7 were corrected by a factor equal to the calculated ratio between the thicknesses of the similar points where strain gage and

DIC measurements were taken. It is possible to see that strains independently measured by both techniques coincided satisfactorily, and this can be demonstrated by the proximity of the data points of a 45° line. The handling of these data revealed an average deviation of  $-8\mu\epsilon$  and a root mean square deviation of  $79\mu\epsilon$ .

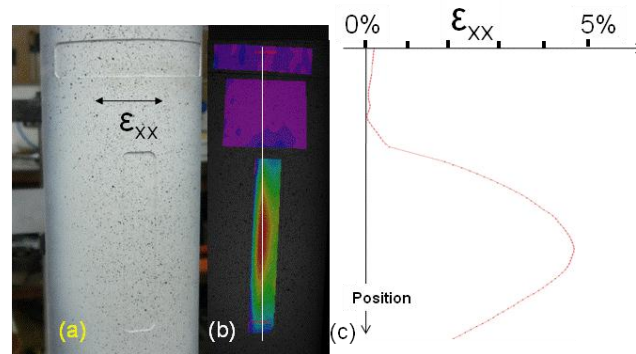


Figure 6: Circumferential strain distribution measured by the DIC technique for points located along a vertical line that crosses the centerline of the circumferential and longitudinal defects; (a) image of the specimen viewed by one of the CCD cameras; (b) image of the strain response given by the VIC-3D 2009 software; (c) strain distribution.

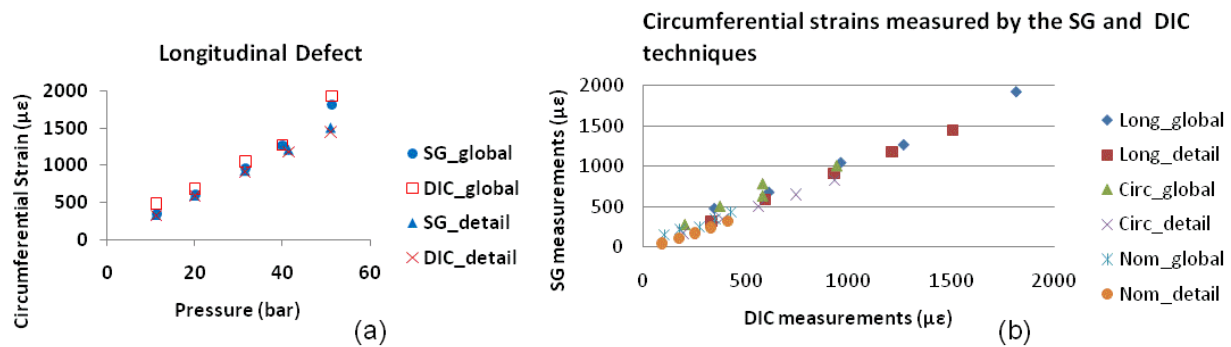


Figure 7: DIC and SG elastic strain measurements collected in the pressure vessel test; (a) circumferential strains at the central point of the longitudinal defect; (b) comparison of DIC and SG measurements at similar points of the specimen.

By means of calculating the angular coefficients (circumferential and longitudinal strains varying with pressure) of the elastic data (as presented in Figure 7a, for example), elastic strain and stress concentration factors ( $K_\epsilon$  and  $K_\sigma$ , respectively) were determined and are given in Table 3. The strain concentration factor  $K_\epsilon$  was calculated by the ratio of the circumferential or longitudinal strain measured at the desired point and the circumferential strain measured by the strain gage positioned in the nominal area of the specimen. This area corresponded to the point of measurement located at the center of the specimen, named R-Nom in Figure 5.

The calculated stress concentration factor  $K_\sigma$  was defined as the ratio of the circumferential or longitudinal stress occurring at the considered point and, respectively, the circumferential or the longitudinal stress occurring at the nominal center point of the specimen. The  $K_\sigma$  calculation used basic elastic equations that relate stresses and strains to allow transforming the elastic strain data into elastic stress data.

Stress concentration  $K_\sigma$  values determined by the DNV and Kastner equations (5) and (6) (and note of Table 3), respectively, for the circumferential and longitudinal stresses occurring in both circumferential and longitudinal defect areas are also presented in Table 3. One can see in Table 3 that the Kastner equation does a good job of predicting the  $K_\sigma$  values determined by the strain gage measurements. On the other hand, values of  $K_\sigma$  calculated using the DNV equation and using the measured data did not agree at all for both longitudinal and circumferential defects. The real reason for this is under investigation, but a reasonable first guess is that the DNV equation was derived to predict plastic collapse of the remaining ligament for ductile materials, not elastic stresses.

Table 3 also presents the prediction of the rupture pressures calculated by the DNV and Kastner equations for the longitudinal defect and for the circumferential defect, as well as the actual rupture pressure. The minimum calculated rupture pressure is the one that corresponds to the longitudinal defect, and it predicts that the failure will be in the longitudinal direction. As expected, the actual rupture location and direction are well represented by this minimum pressure. The actual rupture pressure was 14.2MPa and its corresponding prediction value given by the DNV equation was 11.7MPa. The DNV pressure value was calculated using the rupture pressure of a pipe specimen without defects, reported in “Caylar (2009)” and reported above to be 22.6MPa, and the strength reduction factor  $(f_R)_c = 1/K_\sigma = 1.96$  furnished in Table 3. The DNV value is 20% (conservative side) smaller than the actual one.



Table 3: Pressure vessel test results

Center point of area of inspection	Direction of strain or stress being assessed	Elastic behavior <sup>1</sup>				Plastic and fracture behavior
		$K_{\epsilon}$ <sup>2</sup>	$K_{\sigma}$ <sup>3</sup>	$K_{\sigma}$ -DNV <sup>4</sup>	$K_{\sigma}$ -Kastner <sup>5</sup>	
Longitudinal defect	Circumferential ( <i>c</i> )	3.18	3.17	1.96	-	Burst pressure (actual)= 14.2MPa
	Longitudinal ( <i>l</i> )	0.38	0.66	-	0.61	
Circumferential defect	Circumferential ( <i>c</i> )	1.81	1.96	1.20	-	Longitudinal defect
	Longitudinal ( <i>l</i> )	0.73	0.96	-	0.62	
Nominal (area located between defects)	Circumferential ( <i>c</i> )	0.90	0.88	- <sup>7</sup>	-	Burst pressure (DNV) <sup>9</sup> = 11.5MPa
	Longitudinal ( <i>l</i> )	0.05	0.97	-	- <sup>7</sup>	Burst pressure (Kastner) <sup>10</sup> = 36.7MPa
Nominal (area located in the center of the specimen)	Circumferential ( <i>c</i> )	1.00	1.00	1.00	-	Burst pressure (Tresca) <sup>11</sup> = 11.5MPa
	Longitudinal ( <i>l</i> )	0.14	0.14	-	0.50 <sup>8</sup>	Circumferential defect Burst pressure (DNV) <sup>9</sup> = 18.8MPa Burst pressure (Kastner) <sup>10</sup> = 36,5MPa Burst pressure (Tresca) <sup>11</sup> = 18.8MPa  Minimum calculated burst pressure (Tresca) = 11.5MPa

Notes

1- Calculations used averaged results determined with the strain gages and DIC techniques and considered the three pressure tests performed under the elastic behavior of the test specimen

2-  $K_{\epsilon}$  = strain concentration factor = ratio of strain (circumferential or longitudinal) measured at the center point of the area of inspection and circumferential strain measured by the nominal rosette located in the center of the specimen  $K_{\epsilon} = \frac{\epsilon_c}{\epsilon_{nom-c}}$  or  $\frac{\epsilon_l}{\epsilon_{nom-l}}$

3-  $K_{\sigma}$  = stress concentration factor = ratio of stress (circumferential or longitudinal) calculated at the center point of area of inspection and circumferential stress calculated at the nominal center point of the specimen. Stresses were calculated using the strain data measured at the respective locations and conditions

$$K_{\sigma} = \frac{\epsilon_c + \mu \cdot \epsilon_l}{(\epsilon_{nom-c} + \mu \cdot \epsilon_{nom-l}) = 1.04} \text{ or } \frac{\epsilon_l + \mu \cdot \epsilon_c}{(\epsilon_{nom-l} + \mu \cdot \epsilon_{nom-c}) = 1.04}$$

4-  $K_{\sigma}$ -DNV = stress concentration factor = ratio of theoretical stress calculated using the DNV equation and theoretical circumferential stress calculated at the center of the specimen, i.e.,  $1/(f_R)_c$ , where  $(f_R)_c$  is given by equation (5)

$$K_{\sigma-DNV} = 1/(f_R)_c$$

5 -  $K_{\sigma}$ -Kastner = stress concentration factor = ratio of theoretical stress calculated using the Kastner equation and theoretical longitudinal stress calculated at the center of the specimen, i.e.,  $1/(f_R)_l$ , where  $(f_R)_l$  is given by equation (6)

$$K_{\sigma-Kastner} = 1/(f_R)_l$$

6- Determined by the DIC technique after bursting the specimen at end of test 4 (see Figure 6)

7- It was assumed a reduction of 10% in the stresses actuating on the nominal area located between the defects.

8- Calculated using the circumferential stress as the nominal theoretical value

9- Calculated by dividing the actual burst pressure of a similar tube without defect (22.6MPa measured in [9]) by the  $K_{\sigma}$ -DNV value of 1.96 or 1.20

10- Calculated by dividing the actual burst pressure of a similar tube without defect (22.6MPa measured in [9]) by the  $K_{\sigma}$ -Kastner value of 0.61 or 0.60

11- Burst pressure (Tresca) = Min (Burst pressure (DNV), Burst pressure (Kastner))

Figure 3 shows the final shape of the pressure vessel specimen at the fracture site (strain gage instrumented area). Figure 6 shows the magnified area of the longitudinal defect that was analyzed by the DIC method. This area is similar to the rupture area but it was kept from fracturing, as expected, due to its much larger remaining thickness. The full field strain analysis of this region is presented in Figure 6 showing the circumferential strain distribution ( $\epsilon_c = \epsilon_{xx}$ ). The central point of the longitudinal defect presents a rather large circumferential strain. The circumferential distribution is compatible with the plot of strains varying with pressure shown in Figure 8. This figure shows the variation of circumferential strains measured by the strain gages under pressure. The values were measured during the fourth (rupture) test. It can be seen that the center of the longitudinal defect (where fracture actually happened) was much more deformed than the other instrumented points. This observation is compatible with the strain plot of Figure 6. Although not shown in this paper, it has to be stated that the measured longitudinal strains at the heavily plastic deformed points were very small when compared to the circumferential strains measured for the same points. This can be seen in the plot of strains shown in Figure 8. The plot presents the circumferential and longitudinal strains measured by the strain gage rosette located in the center of the longitudinal defect. The strains were measured during test four before rupture occurred and show the elastic-plastic behavior of the material point. One can see that the longitudinal strain is very small when compared to the circumferential strain. One can also see that it changes its positive increasing trend after plastic behavior starts. This behavior has been observed before in “Freire et al. (2011)” and it is explained by the restriction offered by the thicker and near walls of the defect, and by a decrease in thickness of this region to guarantee plastic strain behavior at volumetric strain equal to zero.

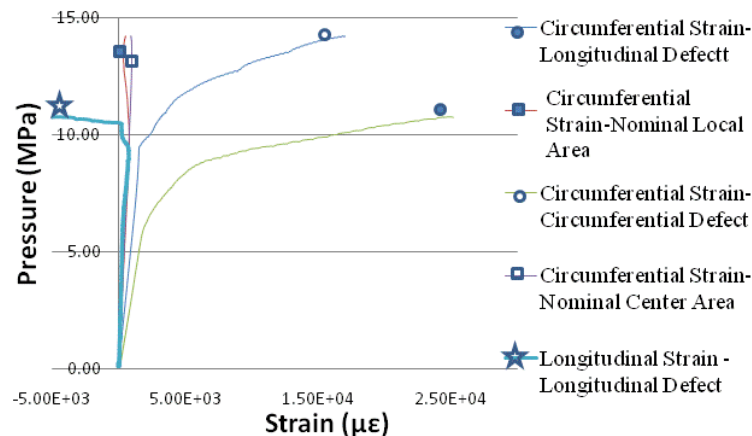


Figure 8: Circumferential and longitudinal strains measured by the strain gage rosette located in the center of the longitudinal defect and circumferential strains measured by the other rosettes located inside the circumferential defect and in the so called nominal-global (center of the specimen) and nominal-detail (between the circumferential and the longitudinal defects) areas.

## 5. CONCLUSIONS

This investigation applied the digital image correlation technique – DIC – to a thin walled cylindrical vessel containing four (two longitudinal and two circumferential) metal loss defects. The DIC has proven to be a good choice for this type of experiment when surface strains have to be measured and elastic and plastic strains are expected. The uncertainty of the DIC technique was addressed by means of testing pressure vessels made of pop-top beverage cans and by comparing DIC results with electrical resistance strain gage measurements. It was concluded that an uncertain uniform state of strain is to be expected. The comparison of strain gage and DIC strains measured at similar points of the pressure vessel tested proved to be satisfactorily close, the average deviation and the root mean square deviation being, respectively,  $-8 \mu\epsilon$  and  $79 \mu\epsilon$ .

The investigation also addressed the calculation of the burst pressures of cylindrical pipes, pipelines and vessels using the equations published by DNV RP F-101 and by Kastner. Results showed that longitudinal elastic strains or stresses occurring in the tested vessel were well predicted by the Kastner equation. Results also showed that the circumferential strains and stresses measured in the experiments were higher than the values predicted by the DNV equation. On the other hand, the actual burst pressure of the vessel tested was conservatively (lower 20%) and reasonably well predicted by the DNV equation.

## 6. REFERENCES

- Anon, 1991, “ASME-B31G - Manual for Determining the Remaining Strength of Corroded Pipelines – A Supplement to ANSI/ASME B31 Code for Pressure Piping”, The American Society of Mechanical Engineers, New York.
- Benjamin, A.C., Freire, J.L.F., Vieira, R.D. and Diniz, J.L.C., 2010 “Burst Tests on Pipeline Containing Circumferential Corrosion Defects”, International Pipeline Conference, IPC2010-31445, 2010.
- Benjamin, A.C., Freire, J.L.F., Vieira, R.D. and Diniz, J.L.C., 2009 “Burst Tests on Pipeline Containing Short Uniform Depth Corrosion Defects”, Rio Pipeline Conference 2009, IBP1105-09, 2009.
- Caylar, P., “Application of a Failure Assessment Diagram to Pipes presenting Dents and Gouges”, Mémoire de Projet d’Expertise, Cooperative Education Program of PUC-Rio & Paris-Tech Art et Métiers – Châlons-en-Champagne, 2009.
- DNV-RP-F101, “Corroded Pipelines”, Det Norske Veritas, Norway, 2004.
- Freire, J.L.F., Benjamin, A.C., Vieira, R.D. and Diniz, J.L.C., “Burst Strength of Pipeline Containing Longitudinal or Circumferential Corrosion Defects”, Proceedings of the Annual Conference on Experimental and Applied Mechanics, Society for Experimental Mechanics, 2011.
- M.A. Sutton, J.J. Orteu, H.W. Schreier, “Image Correlation for Shape, Motion and Deformation Measurements”, Springer Science+Business Media, LLC, 233 Spring Street, New York, NY 10013, USA, 2009.
- Satoru Yoneyama, Go Murasawa, (2009), “Digital Image Correlation”, in Experimental Mechanics, [Ed. Jose Luiz de França Freire], in Encyclopedia of Life Support Systems (EOLSS), Developed under the Auspices of the UNESCO, Eolss Publishers, Oxford, UK, [http://www.eolss.net].
- Shukla, A. and Dally, J.W., “Experimental Solid Mechanics”, College House Enterprises, LLC, 5713 Glen Cove Drive, Knoxville Tennessee, USA, 2010.
- W., Kastner, E., Rohrich, W. Schmitt and R., Steinbuch, 1981, “Critical crack sizes in ductile piping”, International Journal of Pressure Vessel & Piping, Vol. 9, pp. 197-219, 1981.

## 7. RESPONSIBILITY NOTICE

The authors are the only responsible for the printed material included in this paper.